

# Further insight into interfacial interactions in nickel/liquid Sn–Ag solder system at 230–350 °C

Divya Taneja<sup>1,2</sup> · Marion Volpert<sup>1</sup> · Fiqiri Hodaj<sup>2</sup>

Received: 27 June 2017 / Accepted: 20 August 2017 / Published online: 24 August 2017  
© Springer Science+Business Media, LLC 2017

**Abstract** Interfacial reactions are investigated between electrochemical deposited Sn-2 wt%Ag alloy and Ni for isothermal heating at various temperature (230–350 °C) and for various time to study initial stages (1–4 min) and latter stages of reaction (15 min–4 h). During the isothermal heating a continuous compound layer of Ni<sub>3</sub>Sn<sub>4</sub> is formed at the interface between liquid Sn–Ag and solid Ni. In this study scallop like morphology with round and smooth surfaces of Ni<sub>3</sub>Sn<sub>4</sub> intermetallic (IMC) layer is observed for shorter time of isothermal holding, which is in fact contradictory to the observations reported by recent studies which describe the morphology of IMC as elongated and faceted needles. For longer reaction times (>1 h) the scallop-like morphology is transformed gradually to a faceted abnormal growth morphology but not elongated structure. The average thickness of the reaction layer is proportional to a power function of the annealing time with an exponent *n* varying from 0.35 to 0.40 and the apparent activation energy for liquid–solid Ni<sub>3</sub>Sn<sub>4</sub> formation was evaluated to be of about 21 kJ mol<sup>-1</sup>. The role of deposition method of Ni and Sn layers on the morphology and the growth kinetics of the reaction layer is discussed. A theoretical analysis of the initial formation and growth of Ni<sub>3</sub>Sn<sub>4</sub> phase at the Ni/Sn interface is also presented.

## 1 Introduction

Solders, substrate materials and their interfacial reaction products play crucial roles in the reliability of the joint assemblies in microelectronic packages because they provide electrical, thermal and mechanical continuity in electronic assemblies [1, 2]. Solders are, as a rule, eutectic Sn-based alloys containing Ag, Cu and small amounts of other elements. Typical soldering (reflow cycle) of a metallic substrate with Sn-based solder alloys takes few minutes and consists of (i) eutectic melting of a solder bump, (ii) reaction of molten solder with the substrate leading to formation of a reaction product and (iii) cooling [3, 4].

Cu is the most common conductor metal utilized in contact with solders owing to its good solderability characteristics. It is well known that the interaction between Sn-based liquid solders and Cu substrate leads to the formation of two intermetallic compounds (IMCs) at the interface: a scallop-shaped η-Cu<sub>6</sub>Sn<sub>5</sub> phase and a thin continuous layer of ε-Cu<sub>3</sub>Sn phase [1, 2]. The formation and growth of η-Cu<sub>6</sub>Sn<sub>5</sub> and ε-Cu<sub>3</sub>Sn IMCs greatly affect the physical properties and especially the mechanical properties of the joints. Indeed, because of the inherent brittle nature and the tendency to generate structural defects [3], very thick IMC layer at the Cu/solder interface may degrade the reliability of solder joints. It was demonstrated that excessive growth of IMCs may promote brittle failure through weakening the solder joint strength, and hence affecting its long-term reliability [4–7].

Commonly, in order to reduce the growth kinetics of IMC layers at the liquid solder/substrate interface, a Ni barrier is introduced between Cu and the solder. Indeed, it is well known from the literature that the growth kinetics of IMC layers at the Ni/liquid Sn based solder is much lower than that at the Cu/solder interface (see for example Ref.

✉ Fiqiri Hodaj  
fhodaj@simap.grenoble-inp.fr

<sup>1</sup> CEA LETI, Minatech Campus, F-38054 Grenoble, France

<sup>2</sup> Univ. Grenoble Alpes, CNRS, Grenoble INP, SIMAP, F-38000 Grenoble, France

[4]). However, the sustained trend of miniaturization and enhancement of functional density in electronic devices led to the use of increasingly dense arrays and fine-pitch interconnections for microelectronic packaging which poses several new challenges to the microelectronic packaging industry [8–11]. For example, for the finer pitch assembly (<10  $\mu\text{m}$ ) the solder thickness is limited (to some micrometers) and thus the IMC thickness formed at substrate/solder interface should also be limited in order to have some liquid solder left after the reflow process. *This means that even for the liquid solder/Ni substrate system the thickness of the IMC layer formed at the interface can become a very critical factor during the reflow process (some minutes of contact time at temperatures varying from about 240 to 250 °C). Thus the control and limitation of the growth kinetics of this layer becomes nowadays a challenging issue.*

In the past two decades, numerous studies have been conducted on the kinetics of interfacial reactions between Ni substrate and liquid Sn-based solder alloys [6, 12–21]. The common conclusion of various studies is that during Ni/liquid Sn-based solder interactions between 230° to 350 °C the only phase that grows at the interface is the  $\text{Ni}_3\text{Sn}_4$  phase.

However, the morphology and the growth kinetics (in particular, the time exponent but also the growth coefficient) of the IMC layer formed at Ni/liquid Sn interface are not clear, as different results are reported by different research groups. The morphology of the  $\text{Ni}_3\text{Sn}_4$  phase has been reported to be whisker-like [6], scallop-like with smooth surfaces (a non-faceted structure) or round edge surface scallops [12–14], scallop-like faceted [12, 13], continuous and relatively uniform layer [15], elongated rod-like shape [16] and needle-shaped [17].

The reported growth kinetic laws follow a power law with exponents  $n$  varying in general from 0.3 [13] to about 0.5 [18–20] and even  $n \approx 0.6$  [20]. While most of the values of the apparent activation energy  $Q$  of  $\text{Ni}_3\text{Sn}_4$  growth kinetics reported in literature are of about 25 to 30  $\text{kJ mol}^{-1}$ , there are also a few reported values much lower ( $Q = 10.7$  [13]) or higher ( $Q = 43.3$   $\text{kJ mol}^{-1}$  [17]) than 25–30  $\text{kJ mol}^{-1}$ .

The techniques used for the diffusion couples are also different: sputtering [6], dipping [20, 21], soldering technique [16, 18, 22], electroplating [17] and isothermal bonding [14].

Most of the studies are performed for longer reaction time ranging from tens of minutes to hours and sometime even weeks. Very few studies are dedicated on earlier stage of reaction. One of the main reason might be the limitation of performing shorter time isothermal heating in the traditional reflow ovens. Recently, two works have been reported in the literature which are dedicated to the study of the early-stage growth characteristics of  $\text{Ni}_3\text{Sn}_4$  IMC at the Ni/liquid Sn interface [16, 17]. Gorlich et al. [16] studied IMC formation by placing molten Sn balls droplets on a hot Ni plate at

250 °C (solder balls and Ni substrate were immersed into a heated flux just before the experiments). In a different approach, Lis et al. [17] performed their near-isothermal experiments at 250 and 300 °C on a temperature-controlled heating plate by using electroplated Ni and Sn layers 15 and 17  $\mu\text{m}$  thick respectively. Authors clearly specify that no IMC layer is observed at the Ni/Sn interface after the electrochemical deposition.

The main conclusions of these studies are as follows:

- i. Gorlich et al. [16] proposed that growth kinetics follows a power law with a time exponent of 1/3 (up to 3 min) followed by two parabolic growth stages for longer holding times. Lis et al. [17] reported an unexpected thickening behaviour for early stages of reaction up to 3 min with high and almost identical IMC parabolic growth rates at 250 °C ( $k = 1.4 \times 10^{-10} \text{ cm}^2 \text{ s}^{-1}$ ) and 300 °C ( $k = 1.8 \times 10^{-10} \text{ cm}^2 \text{ s}^{-1}$ ). Afterwards the growth kinetics remarkably decreased for both 250 °C ( $2.3 \times 10^{-11} \text{ cm}^2 \text{ s}^{-1}$ ) and 300 °C ( $5.6 \times 10^{-10} \text{ cm}^2 \text{ s}^{-1}$ ).
- ii. After only 1 min of contact between liquid Sn and Ni at 250 °C, an elongated and faceted needles like morphology of  $\text{Ni}_3\text{Sn}_4$  layer is formed at the interface and the reported average thicknesses of the layer obtained are very different: 1.35  $\mu\text{m}$  for Ref. [16] and 3.6  $\mu\text{m}$  for Ref. [17]. Moreover, a very high average aspect ratio  $r$  (=IMC length/IMC width) is reported in both studies:  $r \sim 3$  for Ref. [16] and  $r \sim 10$  for Ref. [17].

Thus, the principal aim of this work is to study the solid/liquid interfacial interactions between electroplated layers of Ni and Sn-2 wt%Ag solder alloy at temperature range of 230–350 °C and for reaction times varying from 1 min to 4 h. Moreover, we compare our experimental results with those reported in the literature and discuss the role of the initial state of the Ni/Sn interface on the morphology and the growth kinetics of the reaction layer in order to elucidate the large discrepancy in the experimental results reported in the literature.

## 2 Experimental procedure

In order to determine the interaction of liquid Sn-2 wt%Ag alloy with Ni, test vehicles were kept under isothermal holding at various temperatures (230, 250, 300 and 350 °C) and time (1–240 min). The test vehicle used for this study is of 3 × 4 mm in size with 92 micropillars 150  $\mu\text{m}$  in diameter which are fabricated by electrochemical deposition. Each micropillar here contains Cu/Ni/Sn-2 wt%Ag. The thickness of Ni and Sn–Ag alloy in each micropillar is 5  $\mu\text{m}$  and 10–25  $\mu\text{m}$  respectively. These pillars are representative of actual interconnects which are formed during the assembly.

The fabrication process used here is a standard electrochemical deposition method described in Fig. 1. It is the most widely used method in the microelectronic industry. As seen in figure, the first fabrication step is to deposit a seed layer which is necessary to provide uniform current distribution for electrodeposition. Following this step, a photoresist is deposited and patterned to define the deposition zone (i.e. Cu/Ni/Sn–Ag pillars). The surface is plasma activated and wafer is immersed in different baths to grow Cu, Ni and Sn–Ag. The growth rate of deposition is controlled by the current density. Various parameters during this deposition step such as current density and the bath chemistry may have an effect on the grain size of deposited layers (see for example [23–25]). Following these steps the photoresist is then stripped and the seed is etched. It is important to note that in some processing steps during the fabrication process, the temperature can go up to 150 °C for cleaning and drying. In the case presented here, the maximum temperature applied was about 70 °C for some minutes.

Experiments for isothermal heating was performed with hot plate. It was first heated at given temperature and then the test vehicle was put on the plate for the given time. All the experiments were performed in ambient atmosphere. After the holding time, the sample were quenched on to the room temperature, by putting them on a cold surface. This is done to ensure that the IMC growth occurs practically just during isothermal holding and not during the heating of the sample from the room to the experimental temperature (near-isothermal conditions). The test vehicle was covered with an aluminium cup to avoid any temperature perturbation due to the surroundings. The accuracy of temperature verified by thermocouple, was found to be  $\pm 2$  °C on the hot plate and  $\pm 5$  °C on the dummy sample (same size as the test vehicle).

After the isothermal holding, cross-section was performed by mechanical polishing, followed by SEM characterization. Then this SEM image was analysed with the help of IMAGEJ software. Using this software, the area of the IMC on the cross-section was measured and the mean IMC thickness is calculated by dividing the measured area of IMC by measured length of the cross-section. The mean length of cross-section for the shorter time experiments was 25  $\mu\text{m}$  and for the longer time experiments was 150  $\mu\text{m}$ . For each case, at least two samples were analysed.

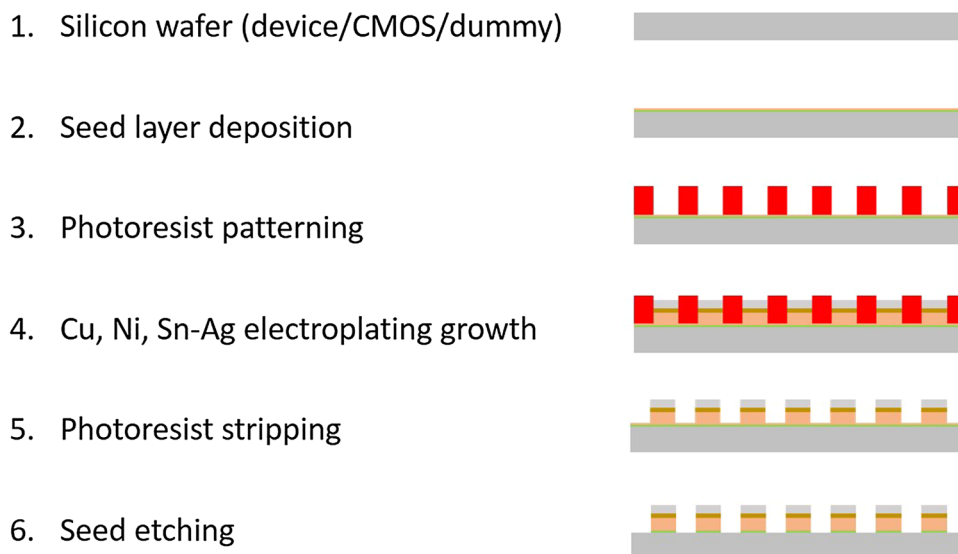
### 3 Results and discussion

In this section, we present and discuss successively: (i) the initial conditions of the Ni/Sn alloy interface before the samples undergo isothermal holdings, (ii) the experimental results on the interactions between liquid alloy and solid Ni at 230–350 °C for annealing times from 1 min to 4 h, (iii) the analysis of the early stages of reaction at liquid Sn/solid Ni interface and (iv) growth kinetics of the  $\text{Ni}_3\text{Sn}_4$  layer at the interface.

#### 3.1 Initial conditions

Figure 2 presents SEM micrographs of the initial state of the Ni/Sn–Ag alloy interface after electroplating process. Figure 2a shows a uniform Sn–Ag alloy layer about 10  $\mu\text{m}$  thick which is deposited on the Ni layer and the interface between the Ni layer and Sn–Ag can be easily seen in Fig. 2b. Also in this figure, a thin and continuous reaction layer can be observed which is formed uniformly at the Ni/Sn–Ag interface. The average thickness of this layer is about 0.25  $\mu\text{m}$ . It is imperative to point out that this result is not in agreement

**Fig. 1** Schematic presentation the fabrication process describing the standard electrochemical deposition method, the most widely used in the microelectronic industry



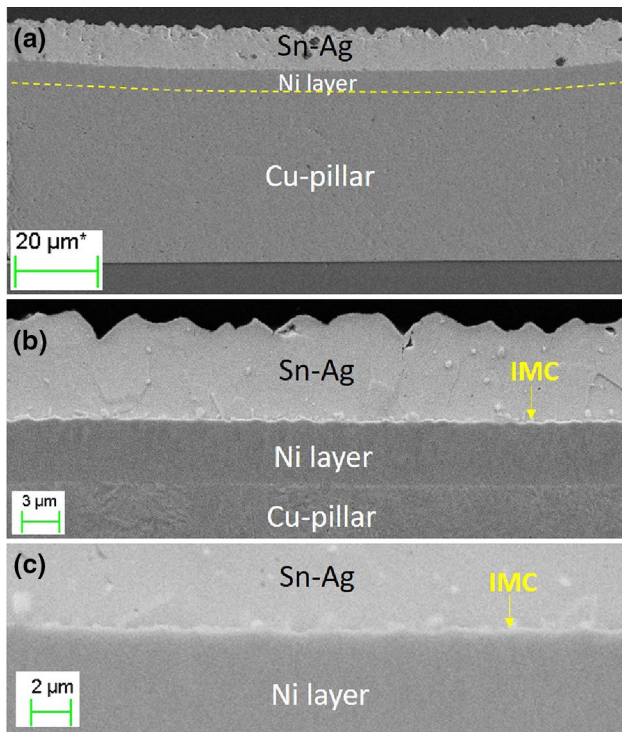
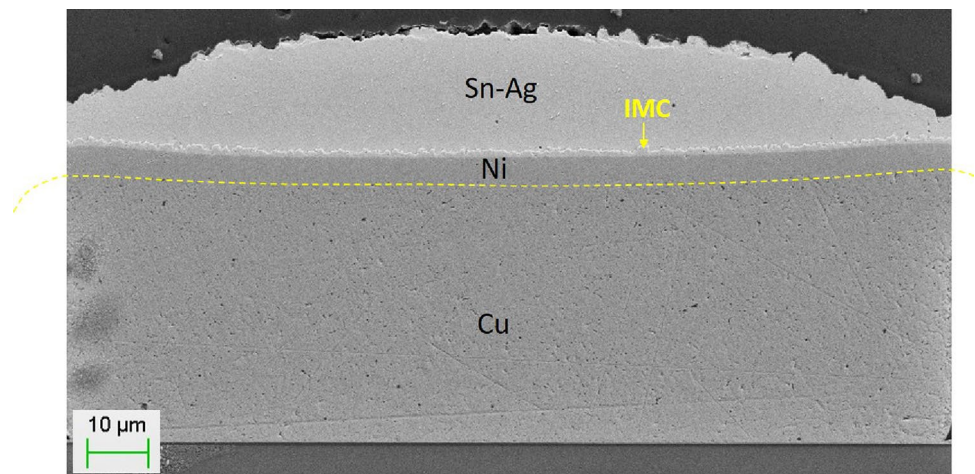


**Fig. 2** SEM micrographs of the initial state of the Ni/Sn–Ag alloy interface after electroplating process

with the recent results of Lis et al. [17] who reported that no intermetallic compound is present at the interface between electroplated 15 μm Ni and 17 μm Sn layers. We believe that this difference is not due to the fact that in our study electroplated Sn-2 wt%Ag alloy is used instead of pure Sn which is used by Lis et al. Given the fact that the Ag–Ni interactions are very weak (no stable Ag–Ni IMC exists) and are much weaker than the Sn–Ag interactions [26], the presence of only 2 wt% of Ag in the deposited Sn–Ag alloy could not affect significantly the Sn–Ni interactions. However, our

**Fig. 3** General view of a sample after an isothermal holding for 1 min at 300 °C showing the formation of a reaction layer about 1 μm thick all over the Ni/Sn–Ag interface



initial condition may be explained by our fabrication process. The grain size, microstructure and density of Ni and Sn may be affected by the electroplating bath composition as well as the current density used, which changes the deposition rate (see for example [23–25]). In addition, after electrodeposition the system undergoes some processing step up to 70 °C as described previously, this combined with storage at room temperature may lead to the formation of a thin layer of IMCs as observed in Fig. 2.

### 3.2 Liquid Sn–Ag/solid Ni interactions

Figure 3 gives a general view of a sample after an isothermal holding for 1 min at 300 °C. This Figure shows that a reaction layer about 1 μm thick is formed all over the Ni/Sn–Ag interface. The average thickness of this layer is practically same everywhere at the interface except the extremities of the sample. It is important to note that after melting, the liquid alloy wets very well the solid Ni (reactive wetting). The contact angle of liquid Sn based alloys on Ni surface is very low (about 20–30° [27, 28]) and the alloy surface forms a spherical cap on Ni surface.

Figure 4 gives some representative SEM micrographs of the reaction product formed at the Ni/liquid Sn–Ag interface for the samples which were aged at 230 to 350 °C for 1, 2, 4 and 15 min. EDX analysis confirmed that the IMC formed at the interface is Ni<sub>3</sub>Sn<sub>4</sub> phase (43 ± 5 at.% Ni and 57 ± 5 at.% Sn). It is in agreement with numerous studies which reported that Ni<sub>3</sub>Sn<sub>4</sub> phase is the only phase that forms and grows at the Ni/liquid Sn interface for temperatures lower than 350 °C.

It is important to note that the interfacial IMC layer exhibits an almost scallop-shaped morphology for various annealing temperature up to 300 °C which is contradictory to what was reported previously. It is interesting that most of the previous studies reported different morphologies of IMC growth and one of the main difference between their

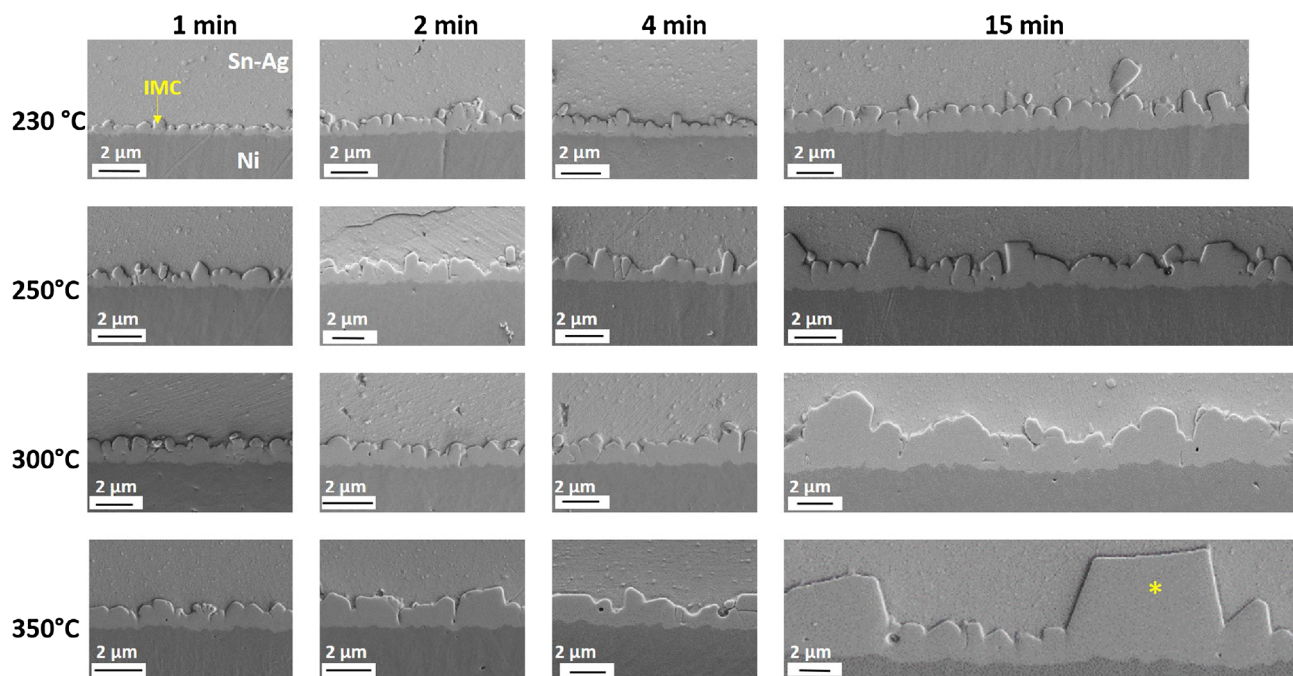


**Fig. 4** Representative SEM micrographs of the reaction product formed at the Ni/liquid Sn–Ag interface for the samples which were aged at 230 to 350 °C for 1, 2, 8 and 15 min

experimental setup was the preparation of diffusion couple. Elongated rod-like shape morphology of IMC was achieved with sessile drop method [16], long, thin, idiomorphic whiskers IMC grew from the diffusion couple which were prepared by sputtering of Ni/Sn [6] and elongated rod-like shape IMC formed when diffusion couple were fabricated by electrochemical deposition [17]. In Sect. 3.3, we will discuss the reason(s) that could lead to this significant difference in the morphology of the interfacial  $\text{Ni}_3\text{Sn}_4$  layer during the first stage of interaction.

Note that the morphology of the  $\text{Ni}_3\text{Sn}_4$  layer formed at the early stage of the Ni/liquid Sn–Ag reaction, seems to be similar to the very well-known morphology of the  $\text{Cu}_6\text{Sn}_5$  layer formed at the Cu/Sn based liquid alloys [29–32]. When the reaction time increases from 1 to 15 min both the width ( $w$ ) and the height ( $h$ ) of the scallops increase and the average ratio  $\rho = h/w$  remains lower than about two. This is slightly lower than the mean value of  $\rho = 2.8 \pm 0.3$  determined by [32] for the scallop-shape  $\text{Cu}_6\text{Sn}_5$  layer formed at the Cu/liquid Sn interface. To the best of our knowledge, one alone study in the literature [22] has reported a scalloped-form morphology of  $\text{Ni}_3\text{Sn}_4$  layer for the early-stages of Ni/liquid Sn reaction (reaction time <5 min). It is worth mentioning that Ghosh et al. [22] have prepared the diffusion couple not by electrochemical deposition (as in our work) but by the sessile drop method of Sn-3.5 wt%Ag on an electroplated Cu/Ni/NiPd/1–3  $\mu\text{m}$  Ni/75 nm Pd (at 230–290 °C, for reaction time 0.5–5 min).

When the reaction time increases up 1 h and more or when the temperature increases up to 350 °C, a significant change in the morphology of the reaction layer is observed: the scalloped-form morphology is progressively replaced by large faceted crystals. This can be clearly seen in Fig. 4 for  $T = 350$  °C and in Fig. 5. These results clearly indicate that an abnormal growth of  $\text{Ni}_3\text{Sn}_4$  crystals occurs when the reaction time increases for a given temperature and/or when the experimental temperature increases for a given reaction time. For example, in the sample  $T = 350$  °C, 15 min, the big crystal (noted\*) has a trapezoidal form in the cross-section plan with large bases length ( $\sim 8$  and  $6 \mu\text{m}$ ) and large height ( $\sim 6 \mu\text{m}$ ) compared to the average thickness of the reaction layer ( $\sim 2.7 \mu\text{m}$ ) measured along 150  $\mu\text{m}$  of the interface. In the sample  $T = 300$  °C, 4 h, the growth of the large crystal (noted\*) is so rapid, compared to other crystals, that the top of the crystal reaches the liquid surface even before the end of the experiment. This result is in good agreement with the findings of Kim et al [33] who reported an abnormal growth of  $\text{Ni}_3\text{Sn}_4$  crystals during Ni/liquid Sn-3.5Ag alloy at 250 °C after 1 h of interaction. In their study, these authors explain the relation between the IMC morphology and the Jackson's parameter [34].

Note that in the sample at  $T = 350$  °C, 4 h, all the solder is consumed thus the average thickness of the reaction layer is lower than the thickness of the layer that would be formed if some solder was left.

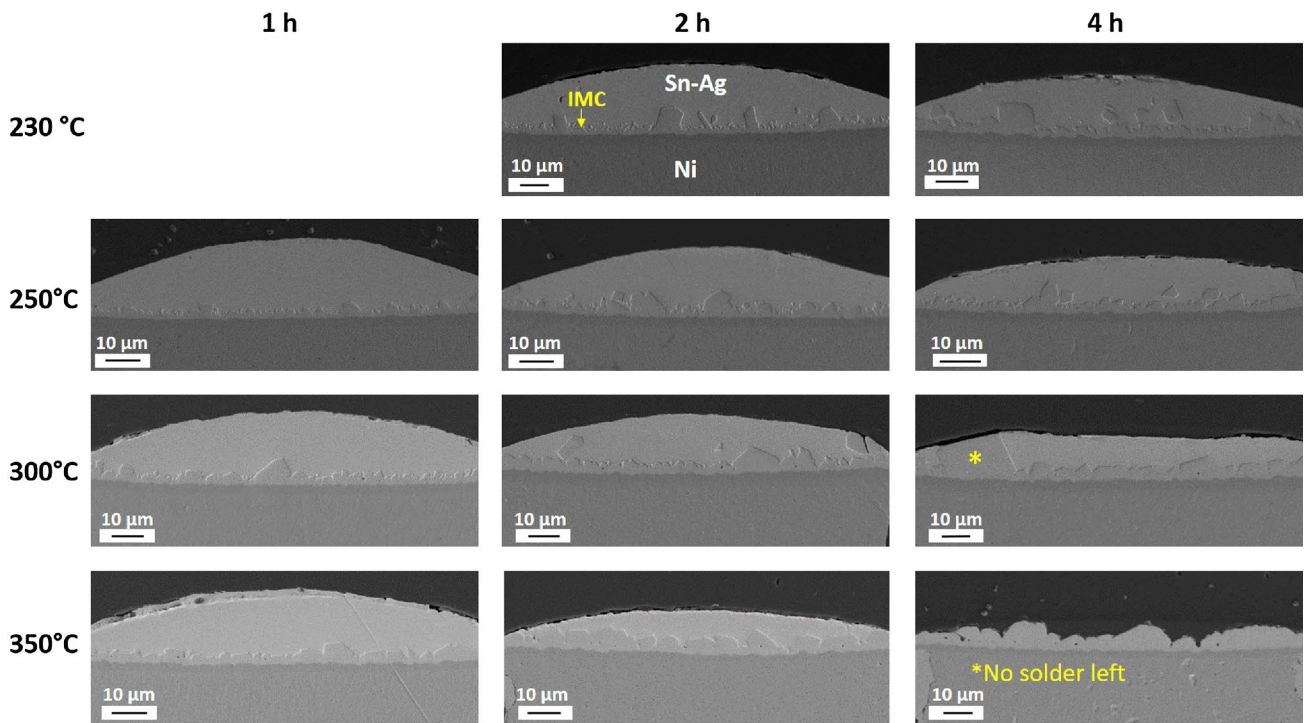


**Fig. 5** Representative SEM micrographs of the reaction product formed at the Ni/liquid Sn–Ag interface for the samples which were aged at 230 to 350 °C for 1, 2, and 4 h

### 3.3 Analysis of Ni<sub>3</sub>Sn<sub>4</sub> growth at the early-stage reaction at liquid Sn/solid Ni interface

The particular scallop-form morphology exhibited by the Ni<sub>3</sub>Sn<sub>4</sub> layer could be attributed to the fact that, in our study, a thin and continuous Ni<sub>3</sub>Sn<sub>4</sub> layer ~0.25 μm thick is already formed at the Ni/Sn–Ag interface by solid state reaction (see Fig. 2b) during fabrication process and/or storage. Thus, when the Sn–Ag alloy is brought to the liquid state, this liquid is not in direct contact with the solid Ni but with the interfacial thin Ni<sub>3</sub>Sn<sub>4</sub> layer already formed.

For this reason, in the following we will first analyse two cases of nucleation and/or growth of Ni<sub>3</sub>Sn<sub>4</sub> phase at Ni/liquid Sn interface when liquid Sn is:

1. In Direct contact with solid Ni and IMC is being formed as a reaction layer between the couple.
2. Not in direct contact with solid Ni due to the pre-existing IMC between the diffusion couple which was formed at the time of fabrication/storage.

Afterwards, we will compare our results with the literature and discuss the growth kinetics of Ni<sub>3</sub>Sn<sub>4</sub> layer during the early-stage of the reaction (<4–5 min).

From a general point of view, the first phase which will form by heterogeneous nucleation at Ni/Sn interface will be the phase with the lower nucleation energy barrier. However,

given the fact that the interfacial energies of the possible phases during nucleation are not known, it is very difficult to predict which phase forms first at the interface. As it is shown by the equilibrium phase diagram of the binary Ni–Sn system (Fig. 6 [35]), the stable phases that can be formed at Ni/Sn interface are Ni<sub>3</sub>Sn, Ni<sub>3</sub>Sn<sub>4</sub> and Ni<sub>3</sub>Sn<sub>2</sub>. It has been demonstrated by numerous studies that, for temperatures lower than 350 °C, the only phase that forms and grows at the Ni/Sn interface is the Ni<sub>3</sub>Sn<sub>4</sub> phase (see Sect. 1), therefore we will consider only Ni<sub>3</sub>Sn<sub>4</sub> phase formation for this study.

#### 3.3.1 The liquid Sn is in direct contact with the solid Ni

If the liquid Sn is put in direct contact with solid Ni (as it was the case in dipping [21] or sessile drop experiments [16]), the interfacial interaction starts with the very fast dissolution of solid Ni in liquid Sn. At this stage, we assume that the solid Ni/liquid Sn interface is at metastable equilibrium as long as no reaction phase is formed at this interface. Ni diffusion concentration profile through the liquid alloy is then established (see Fig. 7).

The concentration of Ni at the interface is given by  $C_1 = C_{\text{liq-Ni}}$  (Fig. 7a) which is corresponding to the metastable equilibrium between liquid Sn and solid Ni.  $C_2 = C_{\text{liq-}\delta}$  represents the concentration of Ni in liquid alloy in stable equilibrium with  $\delta$ -Ni<sub>3</sub>Sn<sub>4</sub> phase. The corresponding

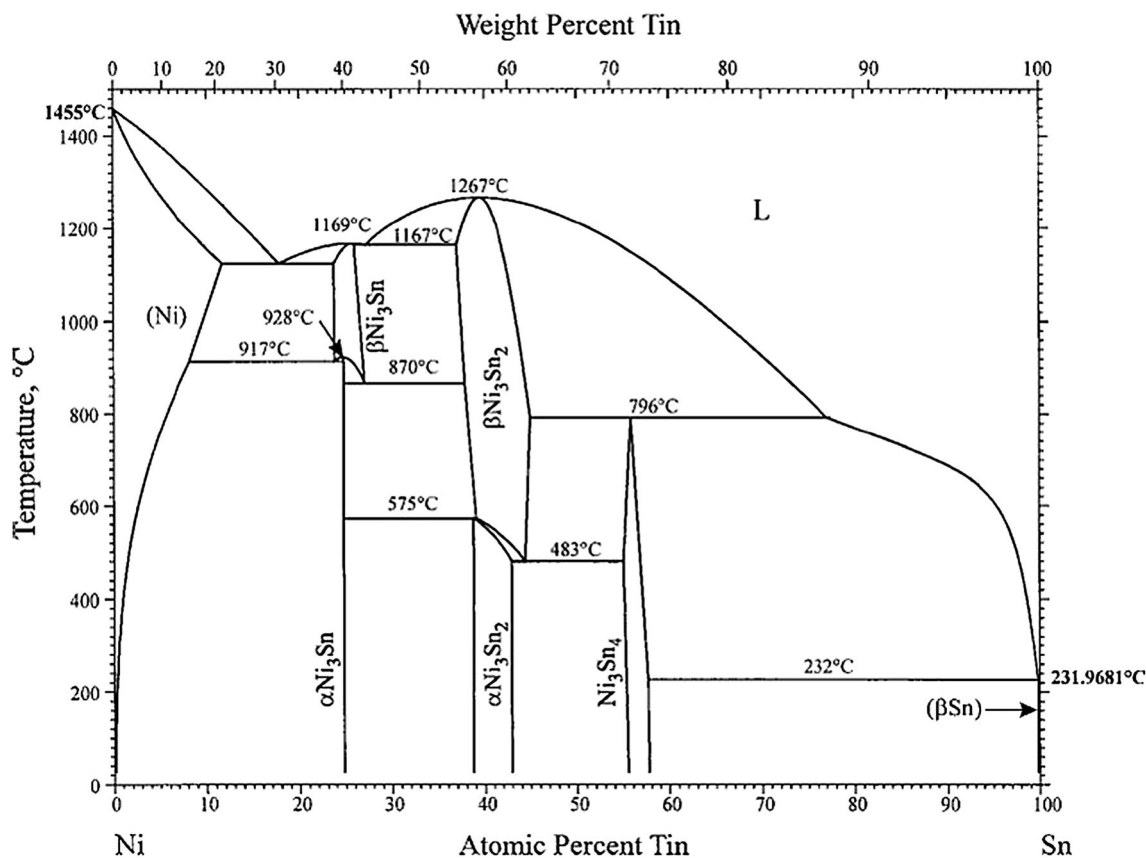


**Fig. 6** Binary Ni–Sn phase diagram [35]

chemical potentials of Ni are indicated by  $\mu_1$  and  $\mu_2$  respectively in Fig. 7c, e.

Figure 7e gives a schematic presentation of the variation of the Ni molar fraction ( $C$ ) with the Gibbs free energy of formation ( $G$ ) of the (Sn, Ni) liquid phase, (Ni, Sn) solid phase and  $\delta$ -Ni<sub>3</sub>Sn<sub>4</sub> compound indicating the stable and metastable equilibria. (As it is already mentioned above, the Ni<sub>3</sub>Sn and Ni<sub>3</sub>Sn<sub>2</sub> phases are not taken into account in Fig. 7). Figure 7e shows in particular the metastable equilibria at the solid/liquid interface and the stable  $\delta$ -Ni<sub>3</sub>Sn<sub>4</sub>/liquid equilibria as well as the corresponding chemical potentials of Ni and Sn.

To qualify the stable and metastable equilibria concentrations, we rely on a CALPHAD modelling of the binary Ni–Sn system published by Liu et al. [36] and Gosh [37]. Given the fact that the diffusion coefficient of Ni in solid Sn at 350 °C is extremely low ( $D_{\text{sol}} \approx 7.10^{-24} \text{ m}^2 \text{ s}^{-1}$ ) [38], several order of magnitude lower than that of Ni in the liquid Sn ( $D_{\text{liq}} = 5.10^{-9} \text{ m}^2 \text{ s}^{-1}$ ) [39]), therefore, we assume that there is no diffusion between solid Sn and Ni and immediately after the melting of Sn (<1 s), the concentration of Ni in the liquid at the liquid/Ni interface reaches  $C_1$ .

The variation of  $C_1$  with the temperature is plotted in Fig. 7e and the calculated values of  $C_1$  and  $C_2$

at  $T = 250\text{--}350$  °C are given in Table 1. This table shows that in the 250–350 °C temperature range  $C_2 \sim 0.7 > C_{\text{Ni}_3\text{Sn}_4} = C_\delta = 4/7 \approx 0.43 >> C_1 \sim 10^{-3}\text{--}10^{-2}$  and the calculated values of  $C_2$  are in good agreement with experimental ones reported in Ref. [40].

As long as no reaction phase is formed at the Ni/liquid alloy interface, the variation of the Ni concentration ( $C$ ) with the time  $t$  and the distance  $z$  from this interface (i.e., diffusion in a semi-infinite medium), is given by the following relation [41]:

$$C(z) = C_1 \left\{ 1 - \text{erf}(z/2\sqrt{Dt}) \right\} \quad (1)$$

where erf is the error function.

As it is shown by the Fig. 7, the driving force of formation of  $\delta$ -Ni<sub>3</sub>Sn<sub>4</sub> phase from reaction of solid Ni and the metastable liquid Sn is given by the segment BA. Under these conditions, after some diffusion time, the nucleation and growth of  $\delta$ -Ni<sub>3</sub>Sn<sub>4</sub> in the supersaturated liquid alloy become thermodynamically possible.

Note that the liquid close to the interface is extremely supersaturated with Ni, i.e. the ratio  $s = C_1/C_2 = 90$  to 330 is much higher than 1—see Table 1 (where  $C_1 = C_{\text{liq-Ni}}$  and  $C_2 = C_{\text{liq-}\delta}$ ). Let  $d$  be the distance at which

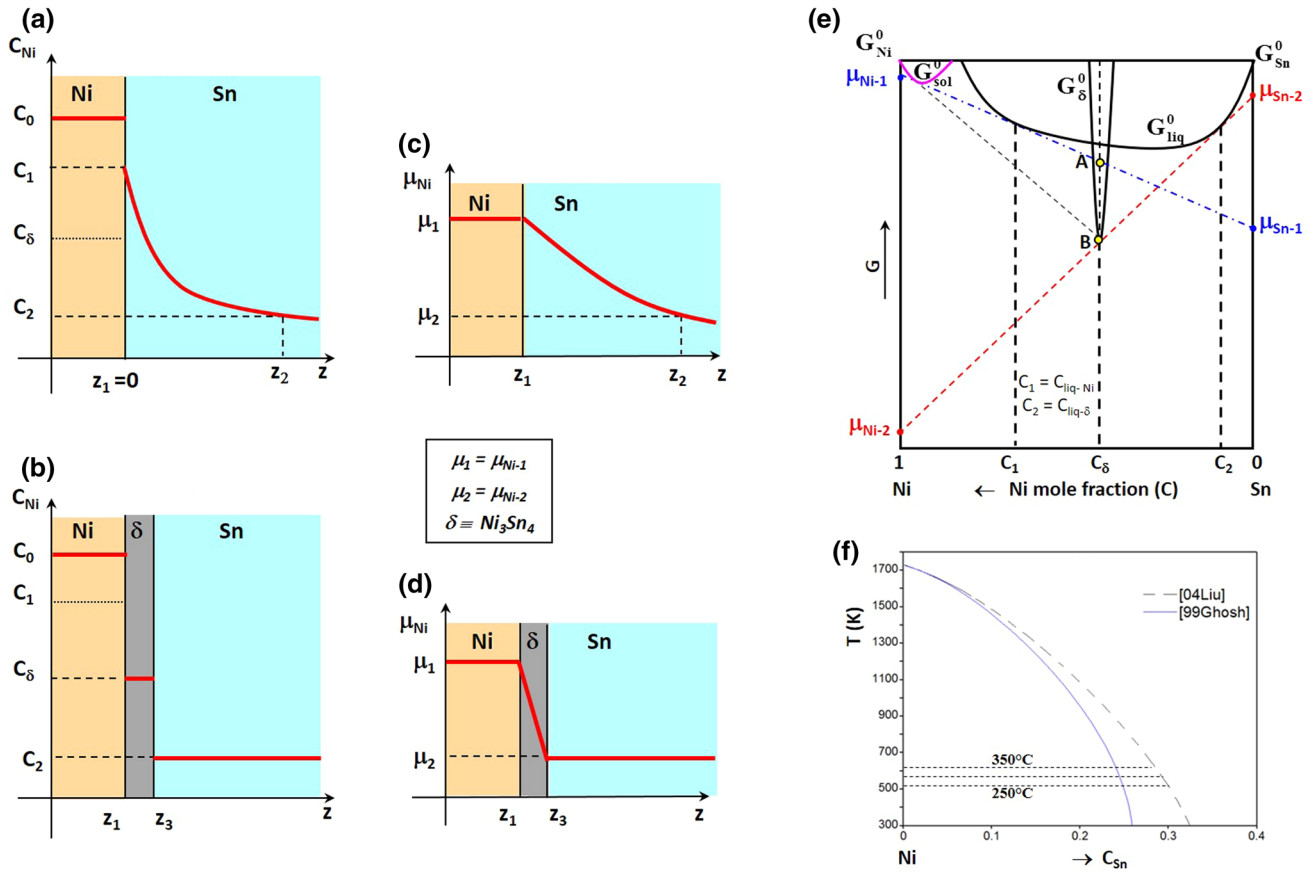


**Fig. 7** Schematic presentation of variation of Ni concentration (a, b) and Ni chemical potential (c, d) through the Ni/liquid Sn interface showing the first instance of contact metastable equilibria between Ni and liquid Sn (a, c) and the formation of the  $\delta$ -Ni<sub>3</sub>Sn<sub>4</sub> phase at the interface (b, d). Schematic presentation of variation of the Gibbs free energy formation of (Sn, Cu) liquid phase, (Cu, Sn) solid phase and

$\delta$ -Ni<sub>3</sub>Sn<sub>4</sub> compound at  $T > 232$  °C indicating the stable (—) and metastable (---) equilibria as well as the chemical potentials of Ni and Sn corresponding to these equilibria (e). Variation with the temperature of the concentration of Ni in liquid Sn at the metastable Ni/liquid Sn equilibrium (f) calculated by CALPHAD modelling of the binary Ni-Sn system using data from Liu et al. [36] and Gosh [37]

**Table 1** Molar fraction of Ni in liquid Sn in equilibrium with Ni<sub>3</sub>Sn<sub>4</sub> phase (stable equilibrium,  $C=C_2$ ) and in equilibrium with solid Ni (metastable equilibrium,  $C=C_1$ ) at 250, 300 and 350 °C values

	250 °C	300 °C	350 °C	Ref.
Molar fraction of Ni in equilibrium with Ni <sub>3</sub> Sn <sub>4</sub> phase (stable equilibrium): $C_2$	$3.75 \times 10^{-3}$	$5.84 \times 10^{-3}$	$8.71 \times 10^{-3}$	[37]
	$2.10 \times 10^{-3}$	$3.68 \times 10^{-3}$	$5.96 \times 10^{-3}$	[36]
Molar fraction of Ni in equilibrium with solid Ni (metastable equilibrium): $C_1$	0.748	0.754	0.759	[37]
	0.697	0.706	0.714	[36]
Degree of supersaturation in Ni = $C_1/C_2$	200	129	87	[37]
	332	192	120	[36]

obtained from CALPHAD modelling of the binary Ni-Sn system using data from Liu et al. [36] and Gosh [37]

the Ni concentration ( $C_d$ ) is equal to the half of that at the Ni/liquid interface, i.e.  $C_d = C_1/2$ . By taking the diffusion coefficient of Ni in liquid Sn at  $T = 250$  °C:  $D = 3 \times 10^{-9} \text{ m}^2 \text{ s}^{-1}$  [39] and typical timescale of nucleation  $t = 10^{-2}$  to 1 s [42], a simple diffusion calculations based on Eq. (1) leads to values of  $d$  varying from 6 to 60  $\mu\text{m}$  approximately.

Thus, a large zone of the liquid phase, some tens of micrometres in width, can be subject to extremely *high supersaturation* (in relation to the formation of Ni<sub>3</sub>Sn<sub>4</sub> compound). Under these conditions, the growth from the supersaturated Sn-Ni liquid solution can lead to the formation of elongated and faceted needles or rod-like shape or long and



thin whiskers of  $\text{Ni}_3\text{Sn}_4$  as it was observed experimentally in [6, 16, 17] respectively.

### 3.3.2 A thin IMC layer is formed at the interface by solid state reaction before Sn melting

Let's consider the second case when a thin and continuous layer of  $\text{Ni}_3\text{Sn}_4$  pre-existed between Ni and Sn—the case of this study (see Figs. 2b, 7b, d). In this case, as soon as Sn is brought in the liquid state, a competition between two processes occurs: (i) dissolution of the  $\text{Ni}_3\text{Sn}_4$  layer in the liquid Sn (which is not saturated with Ni) and (ii) growth of  $\text{Ni}_3\text{Sn}_4$  layer by interdiffusion process through this layer.

The general equations describing the effect of dissolution on the growth rate of a chemical compound layer are described in detail in Ref. [43]. However, the description of the evolution of such a system depends, among other thermodynamic and kinetic factors, on the dissolution rate constant  $k_d$  of reaction compound on the liquid alloy. Unfortunately, data for  $k_d$  are very rare in literature and cannot be estimated by theoretical models making thus difficult the description of the theoretical evolution of such systems [43].

Note however that in our case we can easily verify if, from a thermodynamic point of view, a layer of  $\text{Ni}_3\text{Sn}_4$  compound of initial thickness  $e_{\text{Ni}_3\text{Sn}_4}^0$  can completely dissolve (or not) in a liquid Sn layer of initial thickness  $e_{\text{Sn}}^0$  ( $\gg e_{\text{Ni}_3\text{Sn}_4}^0$ ). This can be verified by performing a mass balance for the nickel. Indeed, knowing the density of Ni, liquid Sn and  $\text{Ni}_3\text{Sn}_4$ :  $\rho_{\text{Ni}} = 8.90 \text{ g cm}^{-3}$ ,  $\rho_{\text{Sn}} = 7.00 \text{ g cm}^{-3}$  and  $\rho_{\text{Ni}_3\text{Sn}_4} = 8.65 \text{ g cm}^{-3}$  [44], one can easily calculate that, the total dissolution of the  $\text{Ni}_3\text{Sn}_4$  layer in liquid Sn leads to a final molar fraction of Ni ( $C_{\text{Ni}}$ ) in liquid Sn given by Eq. (2) :

$$C_{\text{Ni}} = 0.68 \frac{e_{\text{Ni}_3\text{Sn}_4}^0}{e_{\text{Sn}}^0} \quad (2)$$

The application of Eq. (2) with  $e_{\text{Ni}_3\text{Sn}_4}^0 = 0.25 \text{ }\mu\text{m}$  and  $e_{\text{Sn}}^0 = 20 \text{ }\mu\text{m}$  leads to an average Ni concentration in liquid Sn:  $C_{\text{Ni}} \approx 0.009$ . This value is higher than the solubility limit of Ni in liquid Sn ( $C_2$ ) in the 230–350 °C temperature range (see Table 1). Thus, if a  $\text{Ni}_3\text{Sn}_4$  layer of 0.25  $\mu\text{m}$  thick is put in contact with a Sn layer of 20  $\mu\text{m}$  thick at 230–350 °C, the final equilibrium state of the system consists in a saturated liquid Sn with Ni in equilibrium with a thin  $\text{Ni}_3\text{Sn}_4$  remaining layer. If in addition the  $\text{Ni}_3\text{Sn}_4$  layer is situated between Ni and liquid Sn, the contribution of Ni to the thickening of  $\text{Ni}_3\text{Sn}_4$  layer by reactive diffusion, reinforces this statement even more.

We can thus conclude that in our case, the initial layer of  $\text{Ni}_3\text{Sn}_4$ , formed at Ni/Sn interface by solid state reaction

during electrodeposition and/or storage, do not dissolve completely in the early-stage of reaction at the Ni/liquid Sn interface. Thus, the direct contact of Ni with liquid Sn is avoided and the growth of  $\text{Ni}_3\text{Sn}_4$  layer will take place by interdiffusion through the initial  $\text{Ni}_3\text{Sn}_4$  layer leading thus to a scallop-form morphology of  $\text{Ni}_3\text{Sn}_4$  layer during the early-stage of Ni/liquid Sn reaction (see Fig. 4).

### 3.3.3 Comparison with other studies of the early-stage growth kinetics of $\text{Ni}_3\text{Sn}_4$ layer

In this section we will discuss the growth kinetics of  $\text{Ni}_3\text{Sn}_4$  layer during the early-stage reaction (<4–5 min) and compare our results with the literature ones.

In our study, the average thickness ( $e$ ) of  $\text{Ni}_3\text{Sn}_4$  layer after 4 min of reaction at 250 °C is about 1.1  $\mu\text{m}$ . This value is much lower than that reported by Gorlich et al. [16] (5.9  $\mu\text{m}$ ) and by Lis et al. [17] (~2  $\mu\text{m}$  after 3 min of reaction). As it is already discussed before, the scallop-form morphology of the reaction layer obtained in this study is very different from those obtained in [16, 17] (elongated and faceted needles or rod-like shape morphology). This drastic change in the morphology of the reaction layer can lead to a significant change on the growth kinetics of this layer and especially if it is limited by the grain boundary diffusion through this layer (as it will be discussed in Sect. 3.4).

The value of  $e = 1.1 \text{ }\mu\text{m}$  is in good agreement with that reported by Ghosh [22] (0.9  $\mu\text{m}$  at 260 °C for 5 min) who observed also a scallop-form morphology of  $\text{Ni}_3\text{Sn}_4$  layer. It is very interesting to note that Ghosh performed diffusion couples by using a Pd layer 75 nm thick deposited between electroplated Ni and Sn. It is of course difficult to predict in what extent the Pd layer influences the initial stages of interactions between Ni and liquid Sn. However, given the experimental results of Ghosh that are similar to ours, it can be assumed that Pd layer prevents the direct contact between Ni and liquid Sn all over the interface until a continuous layer of  $\text{Ni}_3\text{Sn}_4$  layer is formed at this interface which is scallop-form similar to our observations. These results strongly suggest that the initial stage of the Ni/Sn interface could play an important role on the initial stage of the reaction kinetics at the liquid Sn/Ni interface.

The formation of very elongated  $\text{Ni}_3\text{Sn}_4$  needles at the first stages of reaction could be a very serious issue while using Ni as a direct contact with the liquid Sn based solder and especially for fine pitch assembly. For example, in the system with fine pitch assembly with Ni/Sn/Ni diffusion couples where the needle shaped IMC is formed with thickness let's say  $h$ , (from one diffusion couple) and the available solder thickness is slightly above 2  $h$ , then due to the IMC growth as reported in Refs. [16, 17], the IMCs will come in contact at some discreet points. This will form a mesh of  $\text{Ni}_3\text{Sn}_4$  IMCs inside the melt. On aging, the Sn in

between the mesh will be consumed through the reaction with Ni and this will lead to a net deficit of material within the mesh, ultimately leading to void formation near the bond mid-plane (see for example Ref. [45]).

Thus, if a continuous and sufficiently thick Ni<sub>3</sub>Sn<sub>4</sub> layer is already formed at the Ni/Sn interface by solid state reaction (see Fig. 2b) during fabrication process and/or storage then the growth of this layer occurs by solid state and/or grain boundary diffusion which prevents formation of elongated and faceted needles or rod-like shape morphology during the initial stages of interfacial reaction.

### 3.4 Growth kinetics of Ni<sub>3</sub>Sn<sub>4</sub> layer

For each sample, the average thickness *e* of the Ni<sub>3</sub>Sn<sub>4</sub> layer is calculated using Image J software (see Sect. 2). The average values of *e* from samples used for each holding temperature and time are given in Table 2. In Fig. 8, the average thickness of each Ni<sub>3</sub>Sn<sub>4</sub> layer is plotted against the reaction time. In order to have a better view of the experimental results, they are plotted in two figures, one for the early stage reaction time (up to 4 min, Fig. 8a) and the other for reaction time up to 240 min (Fig. 8b).

**Table 2** Average thickness *e* of the Ni<sub>3</sub>Sn<sub>4</sub> layer formed at liquid Sn-2 wt%Ag alloy/solid Ni interface for different holding temperatures and reaction times

Time (min) →	1	2	4	16	60	120	240
230 °C	0.72	0.88	0.98	1.39		3.51	4.27
250 °C	0.78	1.10	1.14	1.74	3.02	4.25	4.87
300 °C	1.19	1.21	1.41	2.32	3.50	5.41	5.87
350 °C	1.29	1.44	1.60	2.72	3.91	5.64	>6.67*

\*All Sn layer was consumed for this experiment

In the following we assume that the growth kinetics of the Ni<sub>3</sub>Sn<sub>4</sub> layer obeys to the classical power law very often used in the literature:

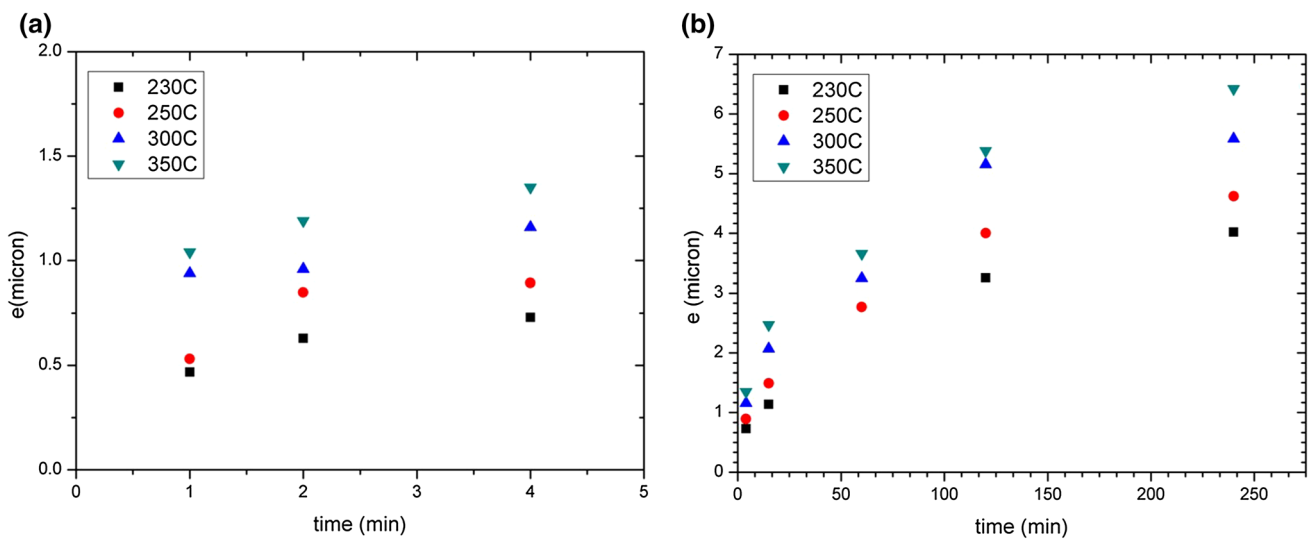
$$\Delta e = e - e_0 = kt^n \tag{3}$$

where *e*<sub>0</sub> and *e* are the thickness of the layer at time *t*=0 and *t* respectively (in our case *e*<sub>0</sub>=0.25 μm) *n* is a growth exponent and *k* the kinetic growth coefficient.

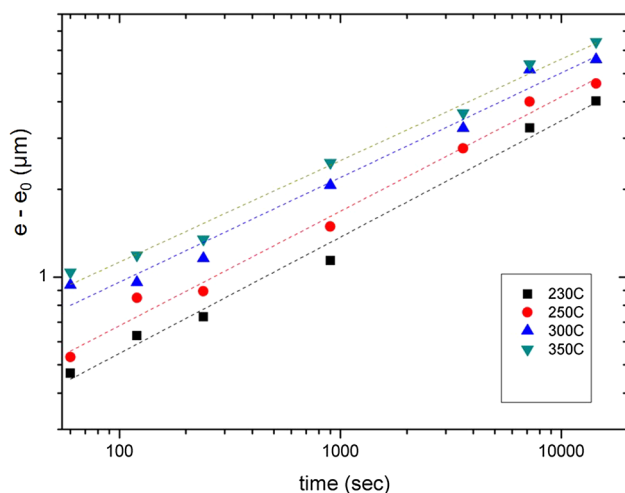
This representation is in relation to the fact that the mechanism of the Ni<sub>3</sub>Sn<sub>4</sub> phase growth in Ni/liquid Sn system is still under discussion. Indeed, the most popular candidates for the power law of Ni<sub>3</sub>Sn<sub>4</sub> phase growth kinetics in the literature are 1/2 and 1/3 [13–17].

Figure 9 shows the log Δ*e* versus log *t* plot of the experimented data. These data are fit with a straight line by linear regression and the obtained values of *k* and *n* values are summarized in Table 3. The values of *n* vary between 0.35 and 0.40 and those of *k* between 0.086 and 0.225 μm s<sup>-n</sup>.

The values of *n* obtained in our study (0.35–0.40) are in good agreement with the recent results of Nakane et al. [14] who studied Ni/liquid Sn by isothermal bonding technique (*n* varying from 0.31 to 0.43) at 260–350 °C. However, it is very surprising to note that the values of



**Fig. 8** Average thickness of Ni<sub>3</sub>Sn<sub>4</sub> layer formed at the Ni/liquid Sn–Ag interface versus reaction time at 230, 250, 300 and 350 °C **a** for short aging times *t*=1–4 min and **b** for long aging times *t*=15–240 min



**Fig. 9** Log–log plot of the variation of  $\Delta e$  with the reaction time at 230, 250, 300 and 350 °C.  $\Delta e = e - e_0$ ,  $e$  and  $e_0$  are the average thickness of  $\text{Ni}_3\text{Sn}_4$  layer formed at the Ni/liquid Sn–Ag interface at time  $t = 0$  and  $t$  respectively (in our case  $e_0 = 0.25 \mu\text{m}$ )

**Table 3** Calculated values the growth constant ( $k$ ) of  $\text{Ni}_3\text{Sn}_4$  layer at liquid Sn-2 wt%Ag alloy/solid Ni interface and of exponent  $n$  [see Eq. (3)] at 230, 250, 300 and 350 °C

T (°C)	230 °C	250 °C	300 °C	350 °C
$n$	0.399	0.393	0.359	0.348
$k (\mu\text{m s}^{-n})$	0.086	0.111	0.183	0.225

$k$  obtained in our study ( $0.086\text{--}0.225 \mu\text{m s}^{-n}$ ) are much lower than those reported by [14] ( $0.268 \mu\text{m s}^{-n}$  at 260 °C and  $7.18 \mu\text{m s}^{-n}$  at 350 °C). Thus the thickness of the  $\text{Ni}_3\text{Sn}_4$  layer observed in our study is systematically about four times lower than that reported in [14], whatever the experimental temperature (from 260 to 350 °C) and the reaction time (from 5 min to 4 h)—compare Fig. 8 with Fig. 5 in [14]. Note that in ref [14], the authors do not discuss in detail the morphology of the reaction layer and only one micrograph of the reaction layer at low magnification is given ( $T = 260 \text{ °C}$ ,  $t = 20 \text{ min}$ ,  $e \approx 7 \mu\text{m}$ , Fig. 1 in Ref. [14]). It seems however from this Figure that the reaction layer exhibits a scallop-like morphology similar to that obtained in our study.

As it has been clearly demonstrated by Gorlich et al. [16], for experiments in this study as well as for all mentioned experiments reported in the literature, the growth kinetics of  $\text{Ni}_3\text{Sn}_4$  layer is so rapid that volume transport through the  $\text{Ni}_3\text{Sn}_4$  layer must be ruled out as a relevant mechanism. Thus the discussion has to focus on the short circuit transport along grain boundary or nanometric liquid channels between  $\text{Ni}_3\text{Sn}_4$  grains, leading thus to a rapid growth rate of this layer [16].

The apparent activation energies ( $Q$ ) of the  $\text{Ni}_3\text{Sn}_4$  layer growth is calculated using the Arrhenius relationship [ $k(T) = k_0 \exp(-Q/RT)$ ] for temperatures ranging from 230 to 350 °C (see Fig. 10), where  $k_0$  is the growth constant of  $\text{Ni}_3\text{Sn}_4$  layer.  $Q$  is evaluated from the slope of the  $\log(k)$  versus  $1/T$  plot using a linear regression analysis giving:  $Q = 21.07 \pm 2.28 \text{ kJ mol}^{-1}$ . This result is in agreement with the values of  $Q$  reported in Refs [12, 14, 18].

The value of  $Q$  reported in these studies ( $20\text{--}30 \text{ kJ mol}^{-1}$ ), is much lower than the activation energies of diffusion process in the bulk intermetallics ( $>100 \text{ kJ mol}^{-1}$  [38]) This result, strongly suggests once again that the growth kinetics of the  $\text{Ni}_3\text{Sn}_4$  layer is not limited by the bulk solid state diffusion through this layer. Owing to the lack of data for activation energy of the grain boundary diffusion in  $\text{Ni}_3\text{Sn}_4$  IMC it is hard to affirm if the growth kinetics of  $\text{Ni}_3\text{Sn}_4$  layer may be limited by the grain boundary diffusion. The activation energy of the grain boundary diffusion in pure Ni and pure Sn is about  $100\text{--}120$  and  $40\text{--}50 \text{ kJ mol}^{-1}$  respectively [38], which strongly suggests that the activation energy of the grain boundary diffusion through the  $\text{Ni}_3\text{Sn}_4$  layer should be higher than  $50 \text{ kJ mol}^{-1}$ , i.e. twice the experimental value obtained in this study. On the contrary, this value is of the same order of magnitude as the activation energy of diffusion in bulk liquid Sn ( $\sim 19 \text{ kJ mol}^{-1}$  [39]), thus the growth kinetics of the  $\text{Ni}_3\text{Sn}_4$  layer could also be limited by the liquid state diffusion through nanometric liquid channels (grain boundaries wetting) as it was suggested for the growth of  $\text{Cu}_6\text{Sn}_5$  layer in the Cu/liquid Sn system [30, 46]. However, this point is out the scope of this study and more experimental work is needed to determine the rate-limiting step during  $\text{Ni}_3\text{Sn}_4$  growth process.

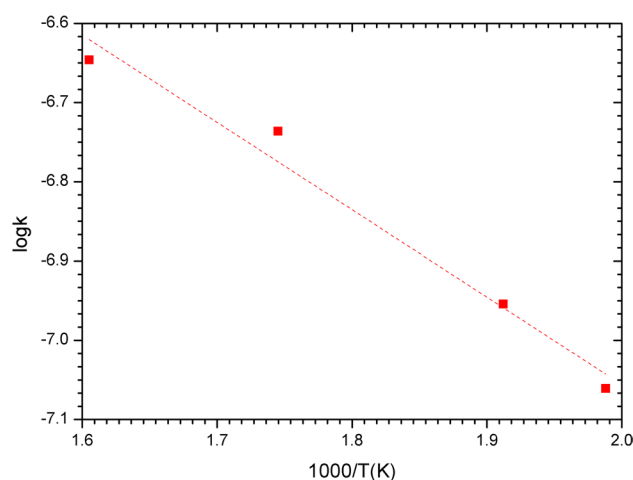


**Fig. 10** Arrhenius plot of  $\text{Ni}_3\text{Sn}_4$  reaction product growth in Sn-2 wt%Ag liquid alloy/solid Ni system  $\log k = f(1/T)$ .  $k$  is the growth constant of  $\text{Ni}_3\text{Sn}_4$  layer in  $\text{m s}^{-n}$  ( $e = k t^n$ ),  $e$  is the layer thickness and  $t$  the reaction time

In general, there is a large discrepancy in the experimental results reported in the literature on the growth kinetics of the  $\text{Ni}_3\text{Sn}_4$  layer for long time experiments (up to 4 h). Just to give a general idea: in this study a thickness of  $\text{Ni}_3\text{Sn}_4$  layer  $e \approx 4.9 \mu\text{m}$ , at  $T = 250 \text{ }^\circ\text{C}$  for  $t = 4 \text{ h}$  is obtained which is in good agreement with  $e \approx 4 \mu\text{m}$  ( $250 \text{ }^\circ\text{C}$ , 4 h) [13] and  $e \approx 3.5 \mu\text{m}$  ( $240 \text{ }^\circ\text{C}$ , 3 h) [15]. On the contrary, in other studies much higher thicknesses are reported:  $e \approx 68 \mu\text{m}$  ( $250 \text{ }^\circ\text{C}$ , 4 h) [16],  $e \approx 16 \mu\text{m}$  ( $260 \text{ }^\circ\text{C}$ , 4 h) [14]. This significant difference in the growth kinetics of the  $\text{Ni}_3\text{Sn}_4$  reaction layer may be due to the microstructure of the reaction layer and in particular to the average grain size. The average grain size of  $\text{Ni}_3\text{Sn}_4$  layer plays an important role in growth kinetics for both growth mechanism (grain boundary diffusion or liquid state diffusion through nanometric liquid channels) [38, 47]. This average grain size of  $\text{Ni}_3\text{Sn}_4$  layer can depend on the grain size of as deposited Ni during solid Ni—liquid Sn reaction. Moreover, given the fact that the  $\text{Ni}_3\text{Sn}_4$  reaction layer can also be sometimes formed and grown by solid state reaction during fabrication process and/or storage (as it was observed in this study), the morphology of this layer can depend not only on the microstructure of both Ni substrate but also on the microstructure of the deposited Sn. Thus, from a practical point of view, it is very important to control the microstructure of the Ni substrate and deposited Sn in order to obtain reproducible results.

## 4 Conclusions

Interfacial reactions between electrochemical deposited Sn-2 wt%Ag alloy and Ni are studied for isothermal holdings at  $230\text{--}350 \text{ }^\circ\text{C}$  and for various time in order to analyse the initial stages (1–4 min) and latter stages of reaction (15 min–4 h).

The main conclusions of this study can be summarized as follows:

- i. A thin  $\text{Ni}_3\text{Sn}_4$  layer about  $0.25 \mu\text{m}$  thick is formed by solid state interaction between Sn and Ni during fabrication process and/or storage at room temperature.
- ii. For short reaction times (1–4 min) a scallop like morphology with round and smooth surfaces of  $\text{Ni}_3\text{Sn}_4$  layer is formed at the interface. The average thickness of this layer is about  $1\text{--}1.5 \mu\text{m}$  after 4 min of reaction.
- iii. From a practical point of view, it is very important to control the initial stages of Ni/liquid Sn interfacial reaction in order to avoid the formation of elongated needles of  $\text{Ni}_3\text{Sn}_4$  phase which can strongly affect the integrity of micrometric sized joints.
- iv. For longer reaction times ( $>1 \text{ h}$ ) the scallop-like morphology is transformed gradually to a faceted abnormal growth morphology but not elongated structure.

The average thickness of  $\text{Ni}_3\text{Sn}_4$  layer is about  $4\text{--}7 \mu\text{m}$  after 4 h of reaction.

- v. The growth kinetics of the  $\text{Ni}_3\text{Sn}_4$  layer follows a power law with exponent  $n$  varying from 0.35 to 0.40 and the apparent activation energy for liquid–solid  $\text{Ni}_3\text{Sn}_4$  formation was evaluated to be of about  $21.07 \pm 2.28 \text{ kJ mol}^{-1}$ . Therefore, the rate controlling step of the growth process can be either the grain boundary diffusion or the liquid state diffusion through nanometric channels inside the  $\text{Ni}_3\text{Sn}_4$  layer.
- vi. A theoretical analysis of the initial formation and growth of  $\text{Ni}_3\text{Sn}_4$  phase at the Ni/Sn interface is presented and the role of the Ni/Sn interactions at the solid state during deposition and/or storage on the morphology and the growth kinetics of  $\text{Ni}_3\text{Sn}_4$  is discussed.

## References

1. K.N. Tu, *Solder Joint Technology: Materials, Properties, and Reliability*. (Springer, New York, 2007)
2. K.N. Tu, *Microelectron. Reliab.* **51**, 517 (2011)
3. K. Zeng, K.N. Tu, *Mater. Sci. Eng. R* **38**, 55 (2002)
4. T. Laurila, V. Vuorinen, J.K. Kivilahti, *Mater. Sci. Eng. R* **49**, 1 (2005)
5. J. Bertheau, F. Hodaj, N. Hotellier, J. Charbonnier *Intermetallics* **51**, 37 (2014)
6. S. Bader, W. Gust, H. Hieber, *Acta Metall. Mater.* **43**, 329 (1995)
7. G. Ghosh, *J. Mater. Res.* **19**, 1439 (2004)
8. D. Taneja, M. Volpert, G. Lasfargues, T. Catelain, D. Henry, F. Hodaj, Understanding the behavior of SnAg bumps at  $10 \mu\text{m}$  pitch and below for imaging and microdisplay application, in *Electronic Components and Technology Conference (ECTC)*, IEEE 66th, 2016, pp. 361–367
9. D. Taneja, M. Volpert, G. Lasfargues, B. Chambion, T. Chaira, A. Vandeneynde, Y. Goiran, D. Henry, F. Hodaj, Cu-SnAg Interconnects Evaluation for the Assembly at  $10 \mu\text{m}$  and  $5 \mu\text{m}$  Pitch, in *Electronic Components and Technology Conference (ECTC)*, IEEE 67th, 2017, in press
10. J. Derakhshandeh, I. De Preter, Relfow process optimization for micro-bumps applications in 3D technology, in *Electronics System-Integration Technology Conference (ESTC)*, 2014, pp. 1–5
11. J.P. Colonna, R. Segaud, F. Marion, M. Volpert, A. Garnier, LDi Cioccio, Y. Beillard, S. Mermoz, F. De Crécy, C. Laviron, S. Chéramy, Towards Alternative Technologies for Fine Pitch Interconnects, in *Electronic Components and Technology Conference (ECTC)*. IEEE 63rd, 2013, pp. 872–878
12. D. Gur, M. Bamberger, *Acta Mater.* **46**, 4917 (1998)
13. J. Shen, Y.C. Chan, S.Y. Liu, *Acta Mater.* **57**, 5196 (2009)
14. A. Nakane, T. Suzuki, O. Minho, M. Kajihara, *Mater. Trans.* **57**, 838 (2016)
15. H.-F. Hsu, S.-W. Chen, *Acta Mater.* **52**, 2541 (2004)
16. J. Gorlich, D. Baither, G. Schmitz, *Acta Mater.* **58**, 3187 (2010)
17. A. Lis, C. Kenel, C. Leinenbach, *Met. Trans. A* **47A**, 2596 (2016)
18. C.-Y. Lin, C.-C. Jao, C. Lee, Y.-W. Yen, *J. Alloys Compd.* **440**, 333 (2007)
19. J. Wang, L.G. Zhang, H.S. Liu, L.B. Liu, Z.P. Jin, *J. Alloys Compd.* **455**, 159 (2008)
20. S.K. Kang, V. Ramachandran, *Scripta Metall.* **14**, 421 (1980)
21. V.I. Dybkov, *Solid State Phenomena* **138**, 153 (2008)

22. G. Ghosh, J. Electron. Mater. **29**, 1182 (2000)
23. A.M. Rashidi, A. Amadeh, Surf. Coatings Technol. **202**, 3772 (2008)
24. A.M. Rashidi, A. Amadeh, Mater. Sci. Technol. **26**, 82 (2010)
25. M.A. Ashworth, G.D. Wilcox, R.L. Higginson, R.J. Heath, C. Liu, R.J. Mortimer, Microelectron. Reliab. **55**, 180 (2015)
26. F.R. de Boer, R. Boom, W.C.M. Mattens, A.R. Miedema, A.K. Niessen, *Cohesion in Metals: Transition Metal Alloys*, 2nd edn. (Elsevier, Amsterdam, 1988)
27. S. Amore, E. Ricci, G. Borzone, R. Novakovic, Mater. Sci. Eng. A **495**, 108 (2008)
28. T. Matsumoto, K. Nogi, Annu. Rev. Mater. Res. **8**, 251 (2008)
29. O. Liashenko, A.M. Gusak, F. Hodaj, J. Mater. Sci. Mater. Electron. **25**, 4664 (2014)
30. O.Y. Liashenko, F. Hodaj, Acta Mater. **99**, 106 (2015)
31. O.Y. Liashenko, S. Lay, F. Hodaj, Acta Mater. **117**, 216 (2016)
32. J. Görlich, G. Schmitz, K.N. Tu, Appl. Phys. Lett. **86**, 053106 (2005)
33. J.H. Kim, S.W. Jeong, H.M. Lee, Mater. Trans. **45**, 710 (2004)
34. K.A. Jackson, J.D. Hundt, Acta Metall. **13**, 1212 (1965)
35. H. Okamoto, J. Phase Equilib. Diff. **27**, 315 (2006)
36. H.S. Liu, J. Wang, Z.P. Jin, Calphad **28**, 363 (2004)
37. G. Ghosh, Met. Trans. A **30**, 1481 (1999)
38. H. Bakker, H.P. Bonzel, *Diffusion in Solid Metals and Alloys*, vol. 26, H. Mehrer (ed.), (Springer, Berlin, 1990)
39. C.H. Ma, R.A. Swalin, Acta Mater. **8**, 388 (1960)
40. P. Nash, A. Nash, Bull. Alloy Phase Diagrams **6**, 350 (1985)
41. J. Crank, *The Mathematics of Diffusion*, 2nd edn. (Clarendon Press, Oxford, 1975)
42. D.M. Herlach, T. Palberg, I. Klassen, S. Klein, R. Kobold, J. Chem. Phys. **145**, 211703 (2016)
43. V.I. Dybkov, *Growth Kinetics of Chemical Compound Layers*, (Cambridge International Science Publishing, 2001) pp. 135–139
44. R.J. Fields, S.R. Low, Physical and Mechanical Properties of Intermetallic Compounds Commonly Found in Solder Joints, in *Metals Science of Joining, Proc. of TMS Symposium*, 1991
45. N.S. Bosco, F.W. Zok, Acta Mater. **52**, 2965 (2004)
46. A.M. Gusak, K.N. Tu, Phys. Rev. B **66**, 115403 (2002)
47. J. Philibert, *Atom movements: diffusion and mass transport in solids (Editions de Physique, Les Ulis, 1991)*